

Counteracting effects operating on Src-homology 2 domain-containing protein tyrosine phosphatase 2 (SHP2) function drive selection of the recurrent Y62D and Y63C substitutions in Noonan syndrome*

Simone Martinelli^{1,8}, Aurelio P. Nardoza^{3,8}, Silvia Delle Vigne¹, Gilda Sabetta⁴, Paola Torrieri², Gianfranco Bocchinfuso⁴, Elisabetta Flex¹, Serenella Venanzi¹, Antonio Paleschi^{4,5}, Bruce D. Gelb⁶, Gianni Cesareni^{3,7}, Lorenzo Stella^{4,5}, Luisa Castagnoli³ and Marco Tartaglia^{1,^}

¹Dipartimento di Ematologia, Oncologia e Medicina Molecolare and ²Centro Nazionale Malattie Rare, Istituto Superiore di Sanità, 00161 Rome, Italy. ³Dipartimento di Biologia and ⁴Dipartimento di Scienze e Tecnologie Chimiche, Università di Roma 'Tor Vergata', 00133 Rome, Italy. ⁵IRCCS Neuromed, 86077 Pozzilli, IS, Italy. ⁶Child Health and Development Institute, Mount Sinai School of Medicine, New York, NY 10029, USA. ⁷IRCCS Fondazione Santa Lucia, 00143, Rome, Italy. ⁸These authors contributed equally to this work.

*Running title: *Counteracting effects of Y62D and Y63C changes on SHP2 function*

[^]To whom correspondence should be addressed: Marco Tartaglia, PhD, Dipartimento di Ematologia, Oncologia e Medicina Molecolare, Istituto Superiore di Sanità, Viale Regina Elena 299, 00161 Rome, Italy, Tel: (+39) 06-49902569; Fax: (+39) 06-49902850; E-mail: mtartaglia@iss.it

Keywords: protein tyrosine phosphatase, SH2 domains, protein structure, signal transduction, genetic diseases, SHP2, Noonan syndrome.

Background: Disease-associated *PTPN11* mutations enhance SHP2's function by destabilizing its inactive state or increasing binding to phosphotyrosyl-containing partners.
Results: Amino acid substitutions at codons 62 and 63 have a profound and complex effect on SHP2 structure and function.

Conclusion: A selection-by-function mechanism acting on mutations at those codons implies balancing of counteracting effects operating on SHP2's activity.

Significance: An unanticipated functional behavior underlies disease-causing weak hypermorphs.

SUMMARY

Activating mutations in *PTPN11* cause Noonan syndrome (NS), the most common non-chromosomal disorder affecting development and growth. *PTPN11* encodes SHP2, a Src homology 2 (SH2) domain-containing protein tyrosine phosphatase that positively modulates RAS function. Here, we characterized functionally all possible amino acid substitutions arising from single-base changes affecting codons 62 and 63 to explore the molecular mechanisms lying behind the largely invariant occurrence of the Tyr62Asp and Tyr63Cys substitutions recurring in NS. We provide structural and biochemical data indicating that the autoinhibitory interaction between the N-SH2 and PTP domains is perturbed in both mutants as a result of an extensive structural rearrangement of the N-SH2 domain. Most mutations affecting Tyr⁶³ exerted an unpredicted disrupting effect on the structure of the N-SH2 phosphopeptide-binding cleft mediating SHP2's interaction with signaling partners. Among all the amino acid changes affecting that codon, the disease-causing mutation was the only substitution that perturbed the stability of SHP2's inactive conformation without severely impairing proper N-SH2's phosphopeptide binding. On the other hand, the disruptive effect of the Tyr62Asp change on the autoinhibited conformation of the protein was balanced, in part, by less efficient binding properties of the mutant. Overall, our data demonstrate that the selection-by-function mechanism acting as driving force for *PTPN11* mutations affecting codons 62 and 63 implies balancing of

counteracting effects operating on the allosteric control of SHP2's function.

Germline missense mutations in *PTPN11* occur in approximately 50% of individuals affected by Noonan syndrome (NS) (1,2), a relatively common developmental disorder characterized by postnatally reduced growth, facial dysmorphism, webbing of the neck, congenital heart defects and hypertrophic cardiomyopathy, skeletal and hematologic anomalies, and variable cognitive deficits (3-5). *PTPN11* encodes SHP2, a widely expressed cytoplasmic protein tyrosine phosphatase that functions as a signal relay protein positively modulating RAS signaling (6). SHP2 is composed of two tandemly arranged N-terminal Src homology 2 (SH2) domains (N-SH2 and C-SH2), a catalytic domain (PTP) and a C-terminal tail with a still not well characterized role. The N-SH2 and C-SH2 domains control SHP2's subcellular localization and functional regulation, with the former acting as an allosteric switch with two spatially non-overlapping sites involved in an intramolecular inhibitory interaction with the PTP domain, and in binding to phosphotyrosyl- (pY-) containing signaling partners (7). Crystallographic data indicate that the catalytically inactive conformation of SHP2 is stabilized by an extensive intramolecular binding network involving exposed residues of the N-SH2 and PTP domains. Upon engagement of the N-SH2 phosphopeptide binding pocket, a conformational change of the domain weakens the auto-inhibiting interdomain interaction, activating the phosphatase.

Previous work by our group and others provided evidence that NS-causing *PTPN11* mutations perturb SHP2's function through distinct molecular mechanisms (8-11). In most cases, lesions affect residues involved in the N-SH2/PTP interdomain binding network that stabilizes SHP2 in its autoinhibited state, and up-regulate SHP2's function by perturbing the switching between the active and inactive conformations, favoring a shift in the equilibrium toward the former. There are, however, mutations affecting residues located far from the N-SH2/PTP interacting surface. Among them, a few involve residues placed in the phosphopeptide-binding cleft of each SH2 domain, and promote a gain of function of the enzyme by increasing binding affinity for pY-containing signaling partners or

alter their binding specificity to those proteins. Of note, there are mutations that affect residues located within the PTP domain contributing to the stability of the catalytically inactive conformation but also participating in catalysis or controlling substrate specificity. For some of these NS-causing defects, biochemical data indicate that those substitutions favor protein activation by promoting dissociation of the N-SH2 and PTP domains without any substantial perturbing effect on catalysis. Other changes affecting the catalytic domain, as those underlying LEOPARD syndrome (LS), a disorder that is clinically related to NS (12), however, have dramatic consequences on SHP2's catalytic function (9,13,14).

Available mutation data strongly support the idea that the specificity in the amino acid substitution is relevant to SHP2's functional dysregulation and disease pathogenesis. A distinct class of activating mutations in *PTPN11* occurs largely as a somatically acquired event with variable prevalence in childhood hematological malignancies (9,15-17). These leukemia-associated mutations exert a differential perturbing effect on SHP2's function, development and hematopoiesis (9,10,18,19). Similarly, among the mutations causing NS and LS, largely invariant amino acid changes are observed for several recurrently affected codons, indicating a specific role for the residue being introduced (9). Such an invariant occurrence of mutations can be ascribed to diverse driving forces, due to either selection-by-function or site-specific increased mutability (11).

Here, by determining the biochemical behavior of all possible substitutions arising from single-base changes affecting codons 62 and 63, we explored the molecular mechanisms lying behind the largely invariant occurrence of the NS-causing Tyr62Asp and Tyr63Cys amino acid changes. We show that the autoinhibitory interaction between the N-SH2 and PTP domains is perturbed in both mutants as a result of an unanticipated extensive structural rearrangement of the N-SH2 domain rather than a consequence of a local effect. Our data also indicate that replacement of Tyr⁶³ has an unexpected disruptive effect on the structure of the N-SH2 phosphopeptide-binding pocket implicated in SHP2's interaction with signaling partners, and that the disease-causing mutation is the only substitution among all possible amino acid

changes at that codon that perturbs the stability of SHP2's inactive conformation without severely impairing proper N-SH2's binding to the phosphopeptide. On the other hand, the Tyr62Asp change is the only substitution at that codon destabilizing the autoinhibited conformation of SHP2, even though such disruptive effect is balanced, in part, by less efficient binding properties of the mutant. Overall, our findings document that the selection-by-function mechanism acting as driving force for mutations affecting codon 62 and 63 implies the existence of counteracting effects operating on the allosteric control of SHP2's function.

EXPERIMENTAL PROCEDURES

Expression Constructs – The full-length human polyHis-tagged *PTPN11* cDNA was cloned in a pET-26b vector (Novagen) using the *HindIII* and *XhoI* restriction sites. The 12 single-base changes resulting in amino acid substitutions at codons 62 and 63 (Table 1) and the c.184_186delTACinsGAG change resulting in the tyrosine-to-glutamic acid amino acid substitution at codon 62 were introduced by site directed mutagenesis (QuikChange Site-Directed Mutagenesis Kit, Stratagene). The polyHis- and GST-tagged N-SH2 domain constructs (residues 6-103) were PCR generated and cloned in the pET-26b (Novagen) and pGEX-2TK (Amersham Biosciences) vectors. For cellular studies, the full-length *PTPN11* cDNA carrying the NS-causing c.184T>G (Tyr62Asp) and c.188A>G (Tyr63Cys) missense mutations were cloned in pcDNA6/V5-HisA (Invitrogen). The coding sequence of all constructs was confirmed by bidirectional sequencing. FLAG-Gab1 and HA-Erk2 constructs had previously been described (20).

ERK Phosphorylation Assay – 293T cells were cultured in Dulbecco's modified Eagle medium (PBI) supplemented with 10% heat-inactivated fetal bovine serum (Euroclone) and 1% penicillin-streptomycin, at 37 °C with 5% CO₂. Constructs were cotransfected with HA-Erk2 and FLAG-Gab1 using *TransIT-LT1* Transfection Reagent (Mirus). ERK phosphorylation status was evaluated in time-course experiments, basally and following EGF (Invitrogen) stimulation (30 ng/ml), as previously described (20). Following overnight incubation with anti-HA antibody (Sigma), immunoprecipitates were collected with protein G-Sepharose (Amersham Pharmacia

Biotech) for 2 h, washed, and analyzed by Western blotting using the anti-phospho-p44/42 MAPK (Thr202/Tyr204) antibody (Cell Signaling). Membranes were then stripped and probed with anti-HA antibody for protein normalization. To evaluate the SHP2-V5, FLAG-Gab1 and Erk2-HA protein levels, 30 μ g of total lysates were immunoblotted with anti-V5 (Invitrogen), anti-FLAG (Sigma) and anti-HA monoclonal (Sigma) antibodies.

Protein Purification – Recombinant proteins were expressed as previously reported (11), using *E. coli* (DE3) Rosetta2 competent cells (Novagen). Following IPTG-induction at 30 °C, harvesting and cell lysis, polyHis-tagged full-length SHP2 proteins and the isolated N-SH2 domains were purified by chromatography, using the Ni-NTA magnetic agarose beads (Qiagen), and stored at -20 °C with 5 mM DTT. GST-tagged N-SH2 domains were purified using the glutathione-Sepharose beads (Amersham Biosciences), and stored at -80 °C with 20% glycerol.

Phosphatase Assays – Catalytic activity of wild-type SHP2 and generated mutants was evaluated *in vitro* using 20 pmol of purified recombinant proteins in a 200 μ l reaction buffer (25 mM HEPES, pH 7.2; 50 mM NaCl; 2.5 mM EDTA; 62.5 mg/ml BSA, 5 mM DTT) supplemented with 20 mM p-nitrophenyl phosphate (pNPP) (Sigma) as substrate, either in basal condition or in presence of the protein tyrosine phosphatase non-receptor type substrate 1 (PTPNS1) biphosphotyrosyl-containing activation motif (BTAM peptide, hereinafter) [GGGGDIT(Yp)ADLNLPKGGKPPAQAAEPNNHTE(Yp)ASIQTS] (Primm), and incubated at 30 °C for 30 min. Reactions were stopped with 0.1 N NaOH. Phosphate release was determined by measuring A_{405} . Amount, purity and integrity of recombinant proteins were assessed using the Protein Assay Kit (Bio-Rad) and Coomassie staining.

Structural Interpretation and Molecular Dynamics Simulations – Electrostatic calculations were performed with the APBS 1.3 program (21), using the protein coordinates of the protein data bank (PDB) entry 2shp (7), and calculating the electrostatic potential generated by the PTP domain (residues 221-524) on the surface of the N-SH2 domain. The linearized Poisson-Boltzmann equation was solved by the automatically-configured sequential focusing multigrid

algorithm, considering a dielectric constant of 2 and 78.54 for the solute and the solvent, respectively, with single Debye-Hückel boundary conditions, a probe radius of 1.4 Å, and a temperature of 300 K.

Molecular dynamics (MD) simulations were performed using GROMACS 4.0.4 (22), with the GROMOS96 ffG43a1 force field (23). Starting coordinates of the N-SH2 domain of human SHP2 were taken from PDB entry 2shp (chain A; residues 2-104) (7). The program DeepView 4.0.1 (24) was used to insert mutations at position 62 or 63. Rotamers with the lowest energy score were selected. The N- and C-termini of the protein were assumed to be charged. Protein was centered in a triclinic box and hydrated with more than 5000 water molecules. The system equilibration was performed by a two-steps energy minimization, first restraining all protein atoms to their positions, and then removing the restraints. Following initial energy minimizations and a 100 ps MD run during which the protein atoms were position restrained, the temperature of solute and solvent was raised to 300 K in a stepwise manner, performing four MD runs, 50 ps each, at different temperatures (50, 100, 200 and 250 K). Electrostatic interactions were calculated using the particle mesh Ewald method, and a 1.2 nm cut-off radius for the real part calculation. Van der Waals interactions were calculated using a cut-off radius (1.2 nm). The simple point charge (SPC) model was used for water (25), and water geometry was constrained with the SETTLE algorithm (26). A Berendsen thermostat, with a coupling constant of 0.1 ps, was applied in all simulations (27), and the reference temperature was set to 300 K, except where stated otherwise. Pressure coupling was applied employing the Berendsen scheme, with a time constant of 1.0 ps, a reference pressure of 1 bar and a compressibility of $4.5 \cdot 10^{-5} \text{ bar}^{-1}$. Bond lengths were constrained with the LINCS algorithm (28). Simulations were run with a 2 fs timestep, and were at least 100 ns long. Translational and rotational motions of the protein were removed by least-square fitting the positions of the C_{α} carbon atoms of the most rigid residues in the protein (residues 6-8, 27-32, 42-46, 52-57, 75-80, and 97-102) to their starting coordinates.

To evaluate the conformational variations of loop DE (residues 60-63), the distance between the center of mass of the DE loop backbone and the center of mass of the backbone of residues 75-77

of helix B was calculated. Root mean square positional fluctuations (RMSF) of C α atoms were calculated according to standard definitions, between 15 and 100 ns. Molecular graphics was obtained with MOLMOL (29) and the Chimera visualization system (30).

Chemical Denaturation Assays – Intrinsic fluorescence spectra were measured on a Fluoromax 2 fluorimeter (Horiba), with 295 nm excitation and 3 nm bandpass. Emission spectra were collected between 305 and 400 nm, and background was subtracted. The protein was dissolved in a 5mM HEPES buffer, 75 mM NaCl (pH 7.2), at a 5 μ M concentration, in a 3x3 mm pathlength cell. Temperature was controlled with a thermal bath to 20.0 \pm 0.1 $^{\circ}$ C. After addition of the chaotropic agent guanidinium chloride (GndCl, Fluka), equilibration of the system was ensured by acquiring multiple spectra until no further changes were observed.

Surface Plasmon Resonance Analysis – Surface plasmon resonance (SPR) measurements were performed using a BIAcoreX instrument (BIAcore Intl. AB) equipped with two flow-cell sensor chips. Biotinylated BTAM peptide (100 μ g/ml) or the monophosphorylated N-terminal portion of that peptide [GGGGDIT(Yp)ADLNLPKGKK] was resuspended in a buffer containing 10 mM HEPES (pH 7.4), 150 mM NaCl, 3 mM EDTA, and 0.005% (v/v) surfactant P20, and injected over a streptavidin-coated sensor chip (SA), at a flow rate of 10 ml/min for 2 min, to obtain an immobilization level of 800 resonance units. The biotin molecule was linked to the N-terminus of the peptide by a stretch of polyglycine. Wild-type and mutant polyHis-tagged N-SH2 domains were resuspended in the same buffer, and applied at a concentration of 500 nM, with a flow rate of 30 ml/min. The amount of protein bound to the sensor chip was monitored by the change in refractive index, given in arbitrary response units (RU), at 25 $^{\circ}$ C, as a function of time. At the end of the sample plug, the buffer was passed over a sensor surface to allow dissociation. The sensor surface was regenerated for the next sample using a 2 μ l pulse of 35 mM NaOH. As a control, no binding was observed when polypeptides were run on the flow-cell sensor chip with immobilized biotin.

Phosphopeptide Array Binding Analyses – Chip arrays used to characterize the N-SH2 recognition specificity consisted of 6,057

thirteenmers, each displaying a phosphorylated tyrosine residue at position 7 (31). One-fourth of these phosphopeptides were retrieved from pELM (32), while the remaining received a high score according to the NetPhos Neural Network predictive algorithm (33). The list of phosphopeptides is available upon request. The library was arranged together with control spots on a glass slide in three identical sub-arrays of 6,400 dots. Control spots included PBS and FLAG-epitope peptides (negative controls), IgG or IgM antibodies (controls for secondary antibody binding), GST protein (positive control for the primary antibody). TAMRA and Cy3 dyes were spotted to facilitate grid orientation. Sixty peptides were spotted in triplicate to verify within-array reproducibility. Following 1 h blocking in 5% BSA-containing PBS, the phosphopeptide arrays were probed with 1 μ g/ml of each GST-tagged N-SH2 domain. After washing, chips were incubated with an anti-GST Cy-5 conjugated antibody (Amersham-Pharmacia), and fluorescence signals were revealed with a Scan-Array Gx Plus instrument (Perkin Elmer). To determine a positive data set of interacting peptides, the fluorescence intensity of each spot was measured, and the median intensity of the three replicated spots was computed for each of the 6,400 phosphopeptides, which were ordered according to their median fluorescence intensity. Peptides whose binding intensities differed from the average intensity by more than 3 standard deviations (z score >3) were considered as “binders”. For each N-SH2 domain, the enrichment in specific residues at the different position flanking the pY was visualized by using Two Sample Logo representations (34).

SPOT synthesis technology was used to synthesize a subset of opportunely selected phosphopeptides on the cellulose membrane, as previously described (35). Membranes were incubated with the N-SH2^{wt}, N-SH2^{Asp62}, and N-SH2^{Asp63} domains expressed as GST-tagged fusion proteins. Binding efficiency and affinity were revealed using an anti-GST antibody conjugated to horseradish peroxidase fluorophore. Signal intensity was quantified and the fold increase (normalized to the signal obtained for the wild-type N-SH2 domain) was plotted. As positive controls, peptides containing the phosphorylated binding motif of GAB1 and PTPNS1 specifically recognized by the SHP2's N-SH2 domain, were

also spotted. Binomial testing and $P < 0.05$ were applied.

RESULTS

Activity of SHP2 mutants. Available published records document that *PTPN11* mutations affecting codons 62 and 63 are a relatively common event among individuals with NS, accounting for approximately 10% of *PTPN11* mutation-positive cases (Table 1). These missense substitutions have not been observed to occur as somatic changes in cancer. At the nucleotide level, a largely invariant occurrence for the c.184T>G transversion (Tyr62Asp) is observed, while the A>G transition at nucleotide 188 (Tyr63Cys) is the only change occurring at this codon reported so far. None of those codons encompasses a CpG dinucleotide. Assuming similar mutation rates for all the possible single-nucleotide substitutions affecting each codon and functional equivalence of the resulting amino acid changes, the frequency of these missense mutations is significantly higher than that expected simply by chance (Tyr62Asp, $p = 2.1 \times 10^{-19}$; Tyr63Cys, $p = 7.3 \times 10^{-53}$), supporting the idea of a selection-by-function mechanism operating on this non-random distribution of amino acid changes affecting both codons.

Tyr⁶² and Tyr⁶³ are located at the PTP-interacting surface of the N-SH2 domain, and lesions affecting these codons were predicted to perturb the equilibrium between the inactive and active conformation of the protein by affecting the stability of the autoinhibitory N-SH2/PTP interdomain interaction (Figure 1) (8,9). Consistent with the predicted activating role of both the NS-causing Tyr62Asp and Tyr63Cys amino acid substitutions, ectopic expression of the V5-tagged SHP2^{Asp62} and SHP2^{Cys63} mutants in 293T cells promoted enhanced ERK phosphorylation upon EGF stimulation, compared to what observed in cells expressing the wild-type protein (Figure 2). To explore the consequences of the Tyr62Asp and Tyr63Cys amino acid changes on SHP2's biochemical behavior and provide an explanation for their largely invariant occurrence in NS, all possible mutants arising from single-base changes affecting those codons, as well as the wild-type protein, were expressed in bacteria, purified and their phosphatase activities were determined *in vitro*, basally and following stimulation with the BTAM peptide previously demonstrated to activate SHP2 (11,36). Under

basal conditions, all but one SHP2 mutants at codon 62 exhibited a relatively low catalytic activity, which was comparable to that observed for the wild-type protein ($V_{max} = 6.8$ pmol/min/pmol), the exception being the NS-causing SHP2^{Asp62} that showed a 2.3-fold increase in substrate dephosphorylation (Figure 3A). The activating effect of the Tyr62Asp substitution was weaker compared with that promoted by the leukemia-associated Glu76Lys change, but consistent with what has previously been described for most NS-causing lesions affecting residues located at the N-SH2/PTP interface (9,10). Following BTAM stimulation, mutants not associated with NS showed either an increase in phosphatase activity comparable to that observed for the wild-type protein (SHP2^{His62}, SHP2^{Cys62}, and SHP2^{Phe62}), or a slightly enhanced catalytic activity (SHP2^{Asn62} and SHP2^{Ser62}) that was, however, significantly lower than that characterizing the NS-causing mutant ($P_{\text{Student's } t \text{ test}} < 0.005$, in all comparisons). Based on the nature of the amino acid change, a trivial interpretation of the perturbing effect of the Tyr62Asp substitution on the stability of the N-SH2/PTP interaction would imply a possible electrostatic repulsive mechanism resulting from the introduction of a charged side chain at the interface of the two domains. Assessment of the *in vitro* phosphatase activity of the SHP2^{Glu62} mutant (c.184_186delTACinsGAG), however, indicated only a moderate activation compared with the disease-causing SHP2^{Asp62} protein, both basally and following BTAM stimulation, suggesting a more complex role for the tyrosine-to-aspartic acid change in perturbing SHP2's function.

Biochemical analysis performed on the panel of generated mutants at codon 63 provided evidence that, with the exception of SHP2^{His63} and SHP2^{Phe63}, which showed activities comparable to the wild-type protein, mutants exhibited a variable increase in their activation basally (Figure 3A), indicating that most mutations at this codon perturbed the stability of the enzyme in its catalytically inactive conformation. Of note, basal phosphatase activity of the NS-causing SHP2^{Cys63} mutant was only 1.6-fold higher than that of the wild-type protein and considerably lower than that characterizing the SHP2^{Asp63} mutant, indicating only a mild destabilizing effect of this substitution on the N-SH2/PTP interdomain interaction. Following BTAM stimulation, however, most

mutants at this codon appeared unresponsive (SHP2^{Asp63}) or poorly responsive (SHP2^{Asn63}, SHP2^{His63} and SHP2^{Ser63}), suggestive of an unpredicted disruptive effect of these amino acid changes on the N-SH2 pocket involved in phosphopeptide binding. In contrast, the NS-causing SHP2^{Cys63} mutant exhibited markedly augmented catalytic activation ($P_{\text{Student's } t \text{ test}} < 0.05$, in comparison to SHP2^{Phe63} and SHP2^{Asp63}; $P_{\text{Student's } t \text{ test}} < 0.002$, in all other comparisons).

The catalytic activity of the NS-causing SHP2^{Asp62} and SHP2^{Cys63} mutants was then measured as a function of BTAM concentration, and compared with a panel of selected proteins (Figure 3B). Both the pathogenetic mutants were significantly more responsive to peptide stimulation than the wild-type protein. Such enhanced responsiveness is predicted to be a direct consequence of the perturbing effect of these lesions on the N-SH2/PTP interaction network, since the “open” conformation implies an enhanced binding affinity for the phosphopeptide (37). While the increased basal activity of these mutants indicates a destabilization of the inactive conformation of the phosphatase, supporting the idea that a shift in the conformational equilibrium is definitely contributing to their higher responsiveness, the possibility that those lesions might perturb the binding properties of the N-SH2 domain due to a concomitant structural rearrangement of the phosphopeptide binding cleft could not be ruled out. Consistent with this hypothesis and the above observations, the basally hyperactive SHP2^{Asp63} protein was essentially unresponsive at all the investigated BTAM concentrations, indicating impaired phosphopeptide binding.

Overall, our data were consistent with a selection-by-function model implicating the destabilization of the N-SH2/PTP interdomain interaction as primary driving force, but highlighted an unexpected counteracting perturbing effect of a subset of mutations affecting residues 62 and 63 on proper SHP2's binding to its signaling partners.

Consequences on N-SH2 domain structure. Both the NS-causing SHP2^{Asp62} and SHP2^{Cys63} mutants were found to be basally activated and exhibited enhanced responsiveness to BTAM stimulation. Structural analyses were performed to understand the molecular mechanism(s) underlying such a hyperactive behavior. As

anticipated, the Tyr62Asp substitution introduces a charged side chain at the interface between the N-SH2 and PTP domains, which might be suggestive for structural stress due to the introduction of electrostatic repulsion between the surfaces of these domains, analogous to what had previously been recognized for the leukemia-associated Glu76Lys amino acid change (37). Poisson-Boltzmann calculations of the electrostatic potential generated by the PTP domain on the N-SH2 surface, however, indicated that the side chain of the aspartic acid is introduced in a region of positive potential generated by several cationic residues, including Lys³⁶⁴ and Lys³⁶⁶ (Figure 1). Based on these considerations, the Tyr62Asp substitution would be expected to generate electrostatic attraction between the two domains, predicting a more steady interdomain interaction, in contrast to the observed biochemical behavior. This apparently conflicting evidence suggested that the Tyr62Asp substitution might lead to a more complex structural rearrangement of the N-SH2 domain, rather than to a mere perturbation of the N-SH2/PTP interaction. This hypothesis was also consistent with the observed impaired or less efficient responsiveness of the majority of mutants at codon 63 to the BTAM peptide, notwithstanding their basal activation, implying a structural adjustment of the phosphopeptide binding pocket of the N-SH2 domain.

To characterize such perturbing effect(s), MD simulations of the isolated N-SH2 domain carrying either the NS-causing amino acid changes or the Tyr63Asp substitution, the latter included as a representative of unresponsive mutants, were carried out. Simulations started from the structure of the N-SH2 domain in the crystal structure of the whole protein in its autoinhibited conformation, in which the blocking loop of the N-SH2 domain (residues 58-62) obstructs the catalytic site of the PTP domain. Notably, the conformation of this loop during the MD trajectories changed significantly in all mutants, undergoing a conformational transition that led it to fold back onto the domain surface (Figure 4A), reducing its spatial distance with the B helix located behind it (Figure 4B). Among the mutants, the structure of N-SH2^{Asp63} was found to be less stable compared with those of the others, as indicated by the higher root mean square (RMS) fluctuations of its C α atoms (Figure 4C). These findings indicated that all mutations induced a significant conformational

rearrangement of the N-SH2 domain, predicted to reduce the ability of its blocking loop to inhibit the catalytic site of the enzyme, which would favor a shift of the equilibrium toward the active shape of the protein. Such an effect, most probably, underlies the increased basal activity of each mutant.

MD simulations also indicated that the structural origin of the perturbing effect promoted by each mutation differed significantly. In the wild-type protein, the tyrosine residue at position 63 participates to the hydrophobic core of the N-SH2 domain that also involves residues Phe⁴¹, Ile⁵⁶, Leu⁶⁵, Phe⁷¹, Ala⁷², Leu⁷⁴ and Leu⁷⁷. While the Tyr63Cys substitution was predicted to disrupt this region creating a cavity in it, the effect of the Tyr63Asp change could be even more radical, because of the insertion of a charged residue in the hydrophobic pocket. Consistent with this observation, during the trajectory of the N-SH2^{Asp63} mutant, the side chain of the aspartic acid moved towards the protein surface to maximize its solvent exposure, leading to a significant distortion of the entire domain structure (Figure 4D). In contrast, the Tyr62Asp mutation introduced a charged side chain in the water-exposed surface of the protein, which would be expected to cause a perturbation in the network of electrostatic interactions within the blocking loop region. In particular, while a stable salt bridge between residues Asp⁶⁴ and Lys⁷⁰ occurred in the wild-type protein, the side chain of Lys⁷⁰ reoriented to interact with both the aspartic acid residues at position 62 and 64 in the mutant. In addition, the Tyr62Asp amino acid change was predicted to introduce a direct repulsion between Asp⁶¹ and Asp⁶², which are located in the blocking loop, contributing to the perturbation of the local structure and dynamics of this region.

To confirm the structural data experimentally, chemical denaturation curves were obtained by measuring the intrinsic fluorescence of each protein, as a function of GndCl concentration (Figure 5). The emission spectra of all mutants were shifted to longer wavelengths compared to that characterizing the wild-type N-SH2 domain, even under non-denaturing conditions, indicating a higher solvent exposure of the single tryptophan residue of the domain. Since this amino acid is located at position 6, which is spatially far from the site of mutations, this effect indicated a constitutive change in the overall

conformation of the N-SH2 domain. In all mutants, the unfolding transition took place at lower GndCl concentrations compared to the wild-type protein, providing further support for a structural disrupting effect of these amino acid changes. As expected, the effect was significantly larger for the N-SH2^{Asp63} mutant, confirming the dramatic structural perturbation predicted by MD simulations on the whole N-SH2 domain, including its phosphopeptide-binding site.

BTAM binding properties. Biochemical and structural data indicated that most mutants at codon 63 were unresponsive or only slightly responsive to the BTAM peptide, suggesting that these lesions could affect peptide binding affinity. To explore further the unpredicted effect of mutations at codons 62 and 63 on N-SH2 domain function, the binding properties of the isolated N-SH2 domains carrying the NS-causing Tyr62Asp and Tyr63Cys changes were compared with those of N-SH2 domains from the apparently unresponsive SHP2^{Asp63} and wild-type proteins using SPR analysis. Following injection of biotinylated BTAM peptide over a streptavidin-coated sensor chip, recombinant proteins were applied at a concentration of 500 nM, and the amount of bound protein was monitored by the change in refractive index, as a function of time. SPR analysis indicated that the N-SH2^{Cys63} mutant had a binding affinity comparable to that observed for the wild-type domain (Figure 6A). On the other hand, consistent with structural and biochemical data, the N-SH2^{Asp63} mutant was almost completely unable to bind the phosphopeptide, providing direct evidence for the disruptive effect exerted by a mutation affecting a residue located in the N-SH2/PTP interacting surface on the phosphopeptide-binding cleft function. The N-SH2^{Asp62} domain exhibited an intermediate behavior, as it retained a significant affinity for the BTAM peptide, although significantly reduced compared to the wild-type domain. These findings were confirmed using the N-terminal portion of the BTAM peptide phosphorylated at the tyrosine residue known to bind specifically the N-SH2 domain of the phosphatase (36) (data not shown).

Consequences on phosphopeptide recognition and binding specificity. Aside from their effect on binding affinity, the predicted structural rearrangement of the N-SH2 domain in mutants at codons 62 and 63 might also perturb

the recognition specificity for pY-containing signaling partners. To explore this possibility, bacterially-expressed wild-type and mutant forms of the N-SH2 domain were challenged against an array of 6,057 pY-containing naturally occurring peptides known or predicted to be phosphorylated *in vivo*. Array binding assays were also performed on the N-SH2 domain carrying the leukemia-associated Glu76Lys amino acid substitution, as representative of the activating mutations acting merely locally to disrupt the stability of the autoinhibitory N-SH2/PTP interdomain interaction (37). Consistent with available published data (11,38-40), the residues of the phosphopeptide that appeared to mediating binding specificity to the wild-type domain were at -2, -1, +1, +2 and +3 from the phosphotyrosine, as shown by the generated sequence logo, which abridges the residue enrichment at each position flanking the phosphotyrosine in the best ligand peptides (Figure 6B). Those positions were found to bear the highest information content also in N-SH2^{Lys76}, N-SH2^{Asp62}, and N-SH2^{Cys63} binding. For each mutant, a pair-wise comparison of phosphopeptide binding profiles was determined by direct comparison of the median fluorescence intensity of each binder with those measured for the wild-type domain. This analysis documented that all the phosphopeptides identified as high-affinity binders for the wild-type domain were also recognized as good ligands of the N-SH2^{Lys76} domain, with an overall correlation coefficient of 0.75. A similar behavior was observed for the N-SH2^{Asp62} and N-SH2^{Cys63} mutants (correlation coefficients equal to 0.76 and 0.80, respectively), providing evidence that both domains retained recognition specificity comparable to that observed for the wild-type counterpart. In contrast, the Tyr63Asp amino acid change was found to substantially perturb both affinity and specificity, as indicated by the relatively small number of shared binders with the wild-type domain (correlation coefficient = 0.27) and a general more promiscuous behavior.

To further investigate these observations, a selected panel of phosphopeptides, which were predicted to represent the high-affinity binders of the wild-type and mutated N-SH2 domains by fitting their sequence consensus motifs, were synthesized by SPOT synthesis technology, and binding properties of the N-SH2^{Asp62} and N-SH2^{Asp63} domains were assayed (Figure 7). In line with our previous findings, the N-SH2^{Asp62} mutant

was found to bind a significantly smaller number of peptides compared to the wild-type domain, suggesting an overall less efficient binding, while the N-SH2^{Asp63} domain displayed substantially different binding preferences from both the N-SH2^{Asp62} and wild-type domain. For the latter, the analysis confirmed a defective binding to the N-SH2 domain-specific PTPNS1 phosphorylated motif as well as to the majority of phosphopeptides inferred to represent efficient binders of the wild-type N-SH2 domain.

DISCUSSION

In this study, we explored the molecular mechanisms involved in SHP2's functional dysregulation caused by missense changes at codons 62 and 63, and characterized the driving force underlying the largely invariant occurrence of the recurrent Tyr62Asp and Tyr63Cys amino acid substitutions causing NS. Structural and biochemical data demonstrated that the two disease causative lesions are the only substitutions promoting a significant upregulation of SHP2's function among all possible changes resulting from a single-base mutation affecting each codon. As observed for other mutations affecting exposed residues located at the interface of the N-SH2 and PTP domains, most mutations at these codons disrupted the autoinhibitory interaction between the two domains. Unexpectedly, the hyperactive behavior of both mutants was found to be the result of a substantial structural rearrangement of the N-SH2 domain that also involved the phosphotyrosine binding pocket mediating SHP2's interaction with signaling partners and was demonstrated to affect the phosphopeptide-binding capability of the domain in a subset of mutants. These findings imply the existence of counteracting effects of these mutations operating on the control of SHP2's function.

SHP2 is regulated by an allosteric switch involving the N-SH2 domain, in which two distinct sites participate in an intramolecular interaction with the PTP domain and in binding to a pY-containing signaling partner (7). These sites function with negative cooperativity and mediate the conformational transition controlling the inactive and active states of the phosphatase (7,41,42). In the absence of a pY-containing partner, SHP2 assumes an autoinhibited state, as evinced *in vitro* by the low phosphatase activity of the unstimulated enzyme, while the N-SH2

domain loses surface complementarity for its binding site on the PTP domain (7) and overall binding affinity with it (43) in its rearranged phosphopeptide-bound state. This model predicts that dysregulation of SHP2's function can result from structural perturbations involving each of the two interactions. Indeed, previous work by our group and others confirmed that different mechanisms are operating at both these N-SH2 sites for NS-causing *PTPN11* mutations (9-11). In most cases, mutations affect the N-SH2/PTP interdomain binding network locally, destabilizing the inactive conformation of the protein. A subset of mutations, however, can act by increasing SHP2's binding affinity for pY-containing partners, or altering binding specificity. Although these mechanisms are distinct molecularly, both are predicted to act by enhancing SHP2 targeting to activated receptors or docking proteins and prolonging this interaction. Coherently with previously published data, this study provided evidence that the invariant NS-causing Tyr62Asp and Tyr63Cys amino acid substitutions perturb the stability of the N-SH2/PTP interaction required to maintain SHP2 in its catalytically inactive conformation. MD analyses, however, unexpectedly indicated that such a perturbing effect did not result from a local, direct consequence of the introduced residues, as previously observed for disease-causing mutations affecting codons 72 and 76 (9,37), but instead from a more complex conformational rearrangement of the whole N-SH2 domain. Specifically, mutations Ala72Val and Glu76Lys were shown to determine a direct destabilization of the N-SH2/PTP interface by introducing interdomain steric clashes (Ala72Val) or electrostatic repulsion (Glu76Lys) (37). The structural consequences of amino acid substitutions affecting codons 62 and 63 are different. The Tyr63Cys change introduces a cavity in the intradomain hydrophobic core involving residues Phe⁴¹, Ile⁵⁶, Cys⁶³, Leu⁶⁵, Phe⁷¹, Ala⁷², Leu⁷⁴ and Leu⁷⁷. As a consequence, the N-SH2 blocking loop, which is inserted in the PTP catalytic cleft in the autoinhibited conformation of SHP2, undergoes a conformational transition that is predicted to perturb interdomain interactions. A similar effect was observed in the Tyr62Asp mutant. In this case, however, the driving force is the perturbation of the pattern of intradomain electrostatic interactions stabilizing the

conformation of the blocking loop involving residues Asp⁶¹, Asp⁶², Asp⁶⁴ and Lys⁷⁰. A general rearrangement of the whole domain is also suggested for the Tyr63Asp mutant, for which fluctuations in the domain structure, including the residues constituting the N-SH2 binding site and the domain core, were observed. In both cases, possible effects on the N-SH2 binding competence was hypothesized since this region is critical also for the conformational transition leading to opening of the phosphopeptide binding cleft (44). Consistent with these predictions, *in vitro* phosphatase and phosphopeptide binding analyses documented that a number of substitutions at codons 62 and 63 significantly perturb proper phosphopeptide binding efficiency and/or specificity. Such an effect dramatically occurred in the Tyr63Asp mutant and, to a lesser extent, in the NS-causing mutant protein carrying the Tyr62Asp substitution.

Multiple lines of evidence indicate that *PTPN11* mutations occurring as a somatic defect in hematologic malignancies have a greater gain-of-function effect than NS causative lesions (5). The present study provides data indicating that, at least for a subset of germline defects, the weaker hyperactive behavior results from a less efficient functional upregulation of the protein, in which two counteracting effects (*i.e.*, destabilization of the inactive state and perturbed phosphopeptide binding properties) occurs. Consistent with this model, structural and biochemical characterization of a large panel of germline *KRAS* mutations has documented that the milder hypermorphic effect promoted by these lesions, compared to that induced by the oncogenic ones, results from a less effective capability of interacting with downstream effectors, as proved by the inability of these proteins to bind RAF1-RBD or RALGDS-RBD efficiently (45). A similar observation has been reported for a recently identified *HRAS* mutant, *HRAS*^{dupGlu37}, associated with Costello syndrome (46), a disorder clinically related to NS. This lesion affects the switch I region of the RAS effector loop, which is required for the interaction with a number of *HRAS*-binding partners, including GAPs, GEFs and effectors. It has been shown that the slightly enhanced signal flow through the MAPK and PI3K cascades promoted by this allele results from a counteracting effect between GAP insensitivity and inefficient binding to effector proteins, including RAF1. Of note, the

finding that *PTPN11* mutations at codons 62 and 63 acting by destabilizing the autoinhibited SHP2 state but also severely affecting proper activation of the phosphatase after stimulation are not observed in the context of NS (or malignancy) documents the requirement of preserved phosphopeptide binding properties for SHP2 function and its functional upregulation. This conclusion is in line with the absence of any developmental defect in mice heterozygous for a Shp2 mutant lacking the majority of the N-SH2 domain, Shp2^{A46-110}, which was demonstrated to be characterized by constitutive enhanced catalytic activity and inability to bind to intracellular signaling partners (47,48).

In conclusion, our findings document that selection-by-function acts as a primary driving force for the largely invariant occurrence of NS-causing mutations involving codons 62 and 63 of SHP2. Our data indicate that missense single-base changes at those codons have a profound and complex effect on SHP2's functional regulation by affecting both the stability of the autoinhibitory interaction between the N-SH2 and PTP domains, but also perturbing the structure and function of the pY-binding cleft. Among these mutations, the recurrent and largely invariant amino acid changes underlying NS are the only substitutions that significantly affect the catalytic inactive SHP2's conformation without perturbing dramatically proper binding of the phosphatase to its phosphorylated signaling partners.

REFERENCES

1. Tartaglia, M., Mehler, E. L., Goldberg, R., Zampino, G., Brunner, H. G., Kremer, H., van der Burgt, I., Crosby, A. H., Ion, A., Jeffery, S., Kalidas, K., Patton, M. A., Kucherlapati, R. S., and Gelb, B. D. (2001) *Nat. Genet.* **29**, 465-468
2. Tartaglia, M., Gelb, B. D., and Zenker, M. (2011) *Best Pract. Res. Clin. Endocrinol. Metab.* **25**, 161-179
3. Allanson, J.E. (2007) *Am. J. Med. Genet. C Semin. Med. Genet.* **145C**, 274-279
4. van der Burgt, I. (2007) *Orphanet J. Rare Dis.* **2**, 4
5. Tartaglia, M., and Gelb, B. D. (2010) *Ann. N.Y. Acad. Sci.* **1214**, 99-121
6. Neel, B. G., Gu, H., and Pao, L. (2003) *Trends Biochem. Sci.* **28**, 284-293
7. Hof, P., Pluskey, S., Dhe-Paganon, S., Eck, M. J., and Shoelson, S. E. (1998) *Cell* **92**, 441-450
8. Tartaglia, M., Kalidas, K., Shaw, A., Song, X., Musat, D. L., van der Burgt, I., Brunner, H. G., Bertola, D. R., Crosby, A., Ion, A., Kucherlapati, R. S., Jeffery, S., Patton, M. A., and Gelb, B. D. (2002) *Am. J. Hum. Genet.* **70**, 1555-1563
9. Tartaglia, M., Martinelli, S., Stella, L., Bocchinfuso, G., Flex, E., Cordeddu, V., Zampino, G., Burgt, I., Palleschi, A., Petrucci, T. C., Sorcini, M., Schoch, C., Foa, R., Emanuel, P. D., and Gelb, B. D. (2006) *Am. J. Hum. Genet.* **78**, 279-290
10. Keilhack, H., David, F. S., McGregor, M., Cantley, L. C., and Neel, B. G. (2005) *J. Biol. Chem.* **280**, 30984-30993
11. Martinelli, S., Torreri, P., Tinti, M., Stella, L., Bocchinfuso, G., Flex, E., Grottesi, A., Ceccarini, M., Palleschi, A., Cesareni, G., Castagnoli, L., Petrucci, T. C., Gelb, B. D., and Tartaglia, M. (2008) *Hum. Mol. Genet.* **17**, 2018-2029
12. Sarkozy, A., Digilio, M. C., and Dallapiccola, B. (2008) *Orphanet J. Rare Dis.* **3**, 13
13. Hanna, N., Montagner, A., Lee, W. H., Miteva, M., Vidal, M., Vidaud, M., Parfait, B., and Raynal, P. (2006) *FEBS Lett.* **580**, 2477-2482
14. Kontaridis, M. I., Swanson, K. D., David, F. S., Barford, D., and Neel, B. G. (2006) *J. Biol. Chem.* **281**, 6785-6792
15. Tartaglia, M., Niemeyer, C. M., Fragale, A., Song, X., Buechner, J., Jung, A., Hählen, K., Hasle, H., Licht, J. D., and Gelb, B. D. (2003) *Nat. Genet.* **34**, 148-150
16. Tartaglia, M., Martinelli, S., Cazzaniga, G., Cordeddu, V., Iavarone, I., Spinelli, M., Palmi, C., Carta, C., Pession, A., Aricò, M., Maserà, G., Basso, G., Sorcini, M., Gelb, B. D., and Biondi, A. (2004) *Blood* **104**, 307-313
17. Tartaglia, M., Martinelli, S., Iavarone, I., Cazzaniga, G., Spinelli, M., Giarin, E., Petrangeli, V., Carta, C., Masetti, R., Aricò, M., Locatelli, F., Basso, G., Sorcini, M., Pession, A., and Biondi, A. (2005) *Br. J. Haematol.* **129**, 333-339
18. Chan, R. J., Leedy, M. B., Munugalavadla, V., Voorhorst, C. S., Li, Y., Yu, M., and Kapur, R. (2005) *Blood* **105**, 3737-3742
19. Schubert, S., Lieuw, K., Rowe, S. L., Lee, C. M., Li, X., Loh, M. L., Clapp, D. W., and Shannon, K. M. (2005) *Blood* **106**, 311-317
20. Fragale, A., Tartaglia, M., Wu, J., and Gelb, B. D. (2004) *Hum. Mutat.* **23**, 267-277
21. Baker, N. A., Sept, D., Joseph, S., Holst, M. J., and McCammon, J. A. (2001) *Proc. Natl. Acad. Sci. USA* **98**, 10037-10041
22. Hess, B., Kutzner, C., van der Spoel, D., and Lindahl, E. (2008) *J. Chem. Theory Comput.* **4**, 435-447
23. van Gunsteren, W. F., Billeter, S. R., Eising, A. A., Hünenberger, P. H., Krüger, P., Mark, A. E., Scott, W. R. P., and Tironi, I. G. (1996) *Biomolecular Simulation: The GROMOS96 Manual and User Guide*, Hochschulverlag AG an der ETH Zurich Press, Zürich, Switzerland
24. Guex, N., and Peitsch, M. C. (1997) *Electrophoresis* **18**, 2714-2723
25. Berendsen, H. J. C., Postma, J. P. M., van Gunsteren, W. F., and Hermans, J. (1981) *Interaction models for water in relation to protein hydration*, in Pullman, B., *Intermolecular forces*, Reidel Publishing Company, Dordrecht
26. Miyamoto, S., and Kollman, P. A. (1992) *J. Comp. Chem.* **13**, 952-962

27. Berendsen, H. J. C., Postma, J. P. M., van Gunsteren, W. F., Di Nola, A., and Haak, J. R. (1984) *J. Chem. Phys.* **81**, 3684-3690
28. Hess, B., Bekker, H., Berendsen, H. J. C., and Fraaije, J. G. E. M. (1997) *J. Comp. Chem.* **18**, 1463-1472
29. Koradi, R., Billeter, M., and Wuthrich, K. (1996) *J. Mol. Graph.* **14**, 51-55
30. Pettersen, E. F., Goddard, T. D., Huang, C. C., Couch, G. S., Greenblatt, D. M., Meng, E. C., and Ferrin, T. E. (2004) *J. Comput. Chem.* **25**, 1605-1612
31. Sacco, F., Tinti, M., Palma, A., Ferrari, E., Nardoza, A. P., Hooft van Huijsduijnen, R., Takahashi, T., Castagnoli, L., and Cesareni, G. (2009) *J. Biol. Chem.* **284**, 22048-22058
32. Diella, F., Cameron, S., Gemünd, C., Linding, R., Via, A., Kuster, B., Sicheritz-Pontén, T., Blom, N., and Gibson, T. J. (2004) *BMC Bioinformatics* **5**, 79.
33. Blom, N., Gammeltoft, S., and Brunak, S. (1999) *J. Mol. Biol.* **294**, 1351-1362
34. Vacic, V., Iakoucheva, L. M., and Radivojac, P. (2006) *Bioinformatics* **22**, 1536-1537
35. Hilpert, K., Winkler, D. F., and Hancock, R. E. (2007) *Nat. Protoc.* **2**, 1333-1349
36. O'Reilly, A. M., Pluskey, S., Shoelson, S. E., and Neel, B. G. (2000) *Mol. Cell. Biol.* **20**, 299-311
37. Bocchinfuso, G., Stella, L., Martinelli, S., Flex, E., Carta, C., Pantaleoni, F., Pispisa, B., Venanzi, M., Tartaglia, M., and Palleschi, A. (2007) *Proteins* **66**, 963-974
38. Songyang, Z., Shoelson, S. E., Chaudhuri, M., Gish, G., Pawson, T., Haser, W. G., King, F., Roberts, T., Ratnofsky, S., Lechleider, R.J., Neel, B. J., Birge, R. B., Fajardo, J. E., Chou, M. M., Hanafusa, H., Schaffhausen, B., and Cantley, L. C. (1993) *Cell* **72**, 767-778
39. Qin, C., Wavreille, A. S., and Pei, D. (2005) *Biochemistry* **44**, 12196-12202
40. Sweeney, M. C., Wavreille, A. S., Park, J., Butchar, J. P., Tridandapani, S., and Pei, D. (2005) *Biochemistry* **44**, 14932-14947
41. Lee, C. H., Kominos, D., Jacques, S., Margolis, B., Schlessinger, J., Shoelson, S. E., and Kuriyan, J. (1994) *Structure* **2**, 423-438
42. Eck, M. J., Pluskey, S., Trub, T., Harrison, S. C., and Shoelson, S. E. (1996) *Nature* **379**, 277-280
43. Dechert, U., Adam, M., Harder, K. W., Clark-Lewis, I., and Jirik, F. (1994) *J. Biol. Chem.* **269**, 5602-5611
44. Guvench, O., Qu, C. K., and MacKerell, A. D. Jr. (2007) *BMC Struct Biol.* **7**, 14
45. Gremer, L., Merbitz-Zahradnik, T., Dvorsky, R., Cirstea, I. C., Kratz, C. P., Zenker, M., Wittinghofer, A., and Ahmadian, M. R. (2011) *Hum. Mutat.* **32**, 33-43
46. Gremer, L., De Luca, A., Merbitz-Zahradnik, T., Dallapiccola, B., Morlot, S., Tartaglia, M., Kutsche, K., Ahmadian, M. R., and Rosenberger, G. (2010) *Hum. Mol. Genet.* **19**, 790-802
47. Qu, C.K., Shi, Z. Q., Shen, R., Tsai, F. Y., Orkin, S. H., and Feng, G. S. (1997) *Mol. Cell. Biol.* **17**, 5499-5507
48. Saxton, T. M., Henkemeyer, M., Gasca, S., Shen, R., Rossi, D. J., Shalaby, F., Feng, G. S., and Pawson, T. (1997) *EMBO J.* **16**, 2352-2364

Acknowledgments—We are indebted to the Fermi and CASPUR Research Centers (Rome) for providing computational resources.

FOOTNOTES

*This work was funded by grants from Telethon-Italy (GGP10020), ERA-Net for research programs on rare diseases 2009 (NSEuroNet), *Programma di collaborazione Italia-USA 2010* (11US/10) and AIRC (IG 13360) to M.T., and by grants from Telethon-Italy (GGP09243) and European Network of Excellence ENFIN to G.C.

^To whom correspondence may be addressed: Marco Tartaglia, PhD, Dipartimento di Ematologia, Oncologia e Medicina Molecolare, Istituto Superiore di Sanità, Viale Regina Elena 299, 00161 Rome, Italy, Tel: (+39) 06-49902569; Fax: (+39) 06-49902850; E-mail: mtartaglia@iss.it.

FIGURE LEGENDS

Figure 1. Structure of SHP2 in its catalytically inactive conformation and location of Tyr⁶² and Tyr⁶³. The N-SH2, C-SH2, and PTP domains of the protein (residues 2-525; PDB entry 2shp, chain A) are shown in blue, green and red, respectively. The signature motif of the PTP active site (orange), N-SH2 blocking loop (cyan), and N-SH2 phosphopeptide binding cleft (according to the X-ray structure of the N-SH2-peptide complex, PDB entry 1aya) (light blue) are also displayed. The side chains of residues Tyr⁶² and Tyr⁶³ are reported in green and yellow, respectively. Residues missing in the experimental crystallographic structure were reconstructed as previously described (21). The inset shows the electrostatic potential generated by the PTP domain on the N-SH2 surface in the catalytically inactive conformation of SHP2. The PTP backbone is reported as a ribbon, and the N-SH2 surface is shown. Red and blue colors indicate negative and positive potential values ranging from -40 kT/e to +40 kT/e, respectively. The side chains of residues Tyr⁶² and Tyr⁶³ are shown as above.

Figure 2. ERK phosphorylation assays. 293T cells were co-transfected with HA-tagged ERK2, Flag-Gab1 and the indicated V5-tagged SHP2 constructs. Following starvation (12 h) and EGF stimulation (30 ng/ml), cells were immunoprecipitated with anti-HA antibody and probed with anti-pERK1/2 or anti-HA antibodies. Aliquots of corresponding cell lysates were probed with anti-V5, anti-HA and anti-FLAG antibodies. Representative blots (above) and mean \pm SD densitometry values (below) of three independent experiments are shown.

Figure 3. Biochemical characterization of SHP2 mutants. (A) *In vitro* phosphatase assay of wild-type SHP2 and all mutants arising from a single-base change at codons 62 and 63. Mutants carrying the Tyr62Glu substitution and the leukemia-associated Glu76Lys change are also shown for comparison. Catalytic activity was measured as pmoles of phosphate released using pNPP as a substrate, basally (white bars) and following stimulation with 10 μ M BTAM peptide (black bars). Values are expressed as mean \pm SD of at least three independent experiments, and are normalized to the basal activity of the wild-type SHP2. Asterisks indicate the recurrent NS-causing amino acid substitutions. (B) *In vitro* phosphatase assay of wild-type SHP2 and mutant proteins as a function of BTAM peptide concentration. Catalytic activity (mean values \pm SD of three independent experiments) was measured as above.

Figure 4. Molecular dynamics simulations. (A) Ribbon representation of the final structures obtained from simulations of the N-SH2 domain for wild-type (WT), Tyr62Asp, Tyr63Cys and Tyr63Asp mutants. The blocking loop (residues 58 to 62) is evidenced in red. (B) Time evolution of the distance between the blocking loop and the B-Helix located behind it during simulations. (C) Root mean square positional fluctuations (RMSF) of the C $_{\alpha}$ atoms of the wild-type (black), Tyr62Asp (red), Tyr63Cys (green) and Tyr63Asp (blue) N-SH2 domains during simulations. Magenta marks indicate residues belonging to the phosphopeptide binding pocket, as previously defined (21). (D) Ribbon representation of two frames extracted from the Tyr63Asp N-SH2 simulation. Asp⁶³ is shown as red sticks. The blue circles indicate the region undergoing the main conformational transitions.

Figure 5. Chemical denaturation of the isolated wild-type and mutant N-SH2 domains, as indicated by the shift in the fluorescence spectrum of Trp⁶. Protein unfolding leads to exposure of the fluorophore to the water environment, resulting in a red shift in the spectrum. Average wavelength was calculated according to the following equation: $\sum_i \lambda_i F_i / \sum_i F_i$, where F represents fluorescence intensity and λ the wavelength at which it was measured. Values are expressed as mean \pm SD of three independent experiments.

Figure 6. Phosphopeptide binding properties of wild-type and mutant N-SH2 domains. (A) Surface plasmon resonance analysis. Sensorgrams of the interaction of the wild-type protein (red) and the Tyr62Asp (blue), Tyr63Cys (cyan) and Tyr63Asp (pink) SHP2 mutants with the biotinylated BTAM peptide. (B) Two Sample Logo representation of the binding recognition specificity of wild-type and

mutant N-SH2 domains. Each logo abridges the residue enrichment at the positions flanking the phosphorylated tyrosine (pY) in the best ligand peptides. At each position of the top diagram, the overall stack height indicates the sequence conservation, while the height of symbols within each stack indicates the relative frequency of the indicated residue. The bottom diagram illustrates the “anti-motif” (*i.e.*, residues that are enriched at each position in the peptide sequences of the negative set) ($P_{\text{Student's } t \text{ test}} < 0.05$). Residue positions are numbered by referring their position to that of the pY. The Pearson correlation coefficient (PCC) between the wild-type N-SH2 domain and each mutant is also shown.

Figure 7. Phosphopeptide recognition specificity in SPOT synthesis assay. Phosphopeptides were synthesized on a cellulose membrane, which was incubated with the indicated N-SH2 domain expressed as a GST-fusion protein. The binding efficiency and affinity was revealed using an anti-GST antibody conjugated to a fluorophore. The intensity of the signal was quantified and the fold increase (assuming the wild-type intensity equal to 1 for each peptide) was plotted in the bar chart.

Table 1. List of the disease-causing amino acid substitutions arising from single-base changes at codons 62 and 63 of the *PTPN11* gene.¹

Affected residue	Nucleotide substitution	Introduced residue	Occurrence (N = 855)	Associated phenotype
Tyr ⁶²	c.184T>A	Asn	1	NS
	c.184T>C	His		
	c.184T>G	Asp	24	NS
	c.185A>C	Ser		
	c.185A>G	Cys	1	- ²
	c.185A>T	Phe		
	c.186C>A	<i>stop codon</i>		
	c.186C>G	<i>stop codon</i>		
	c.186C>T	<i>silent change</i>		
Tyr ⁶³	c.187T>A	Asn		
	c.187T>C	His		
	c.187T>G	Asp		
	c.188A>C	Ser		
	c.188A>G	Cys	67	NS
	c.188A>T	Phe		
	c.189T>A	<i>stop codon</i>		
	c.189T>C	<i>silent change</i>		
	c.189T>G	<i>stop codon</i>		

¹Data are from the database reported by Tartaglia and co-workers (9) updated to April 2011. The complete list of somatically acquired and germline transmitted disease-causing *PTPN11* mutations and relevant references are available upon request.

²This amino acid change was documented to be germline transmitted in a subject with neuroblastoma without clinical features supporting a diagnosis of NS, suggesting it might represent a private variant causally unrelated to disease. Parental DNAs were not available to verify the *de novo* occurrence of this variant.

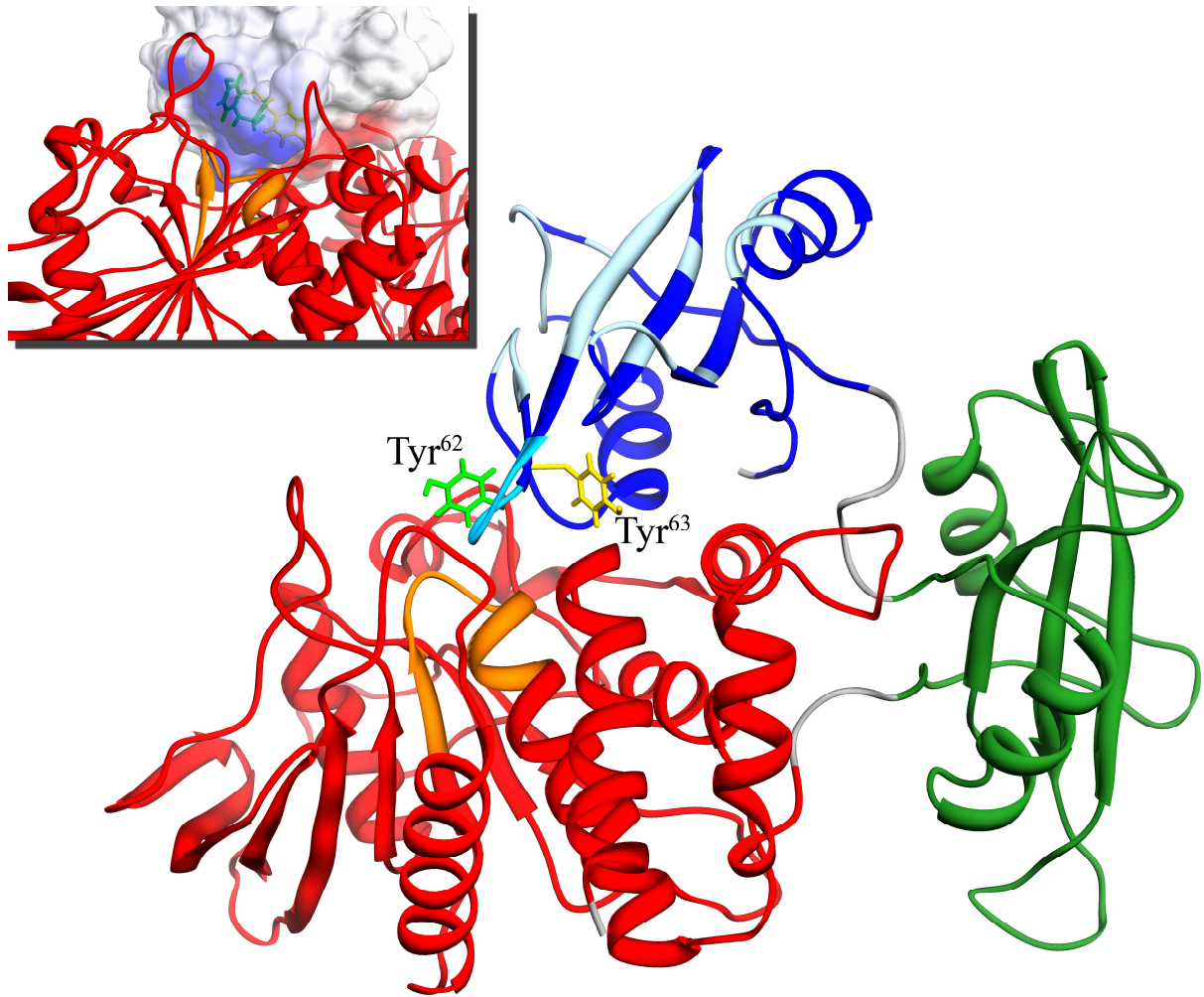


Figure 1. Structure of SHP2 in its catalytically inactive conformation and location of Tyr⁶² and Tyr⁶³.

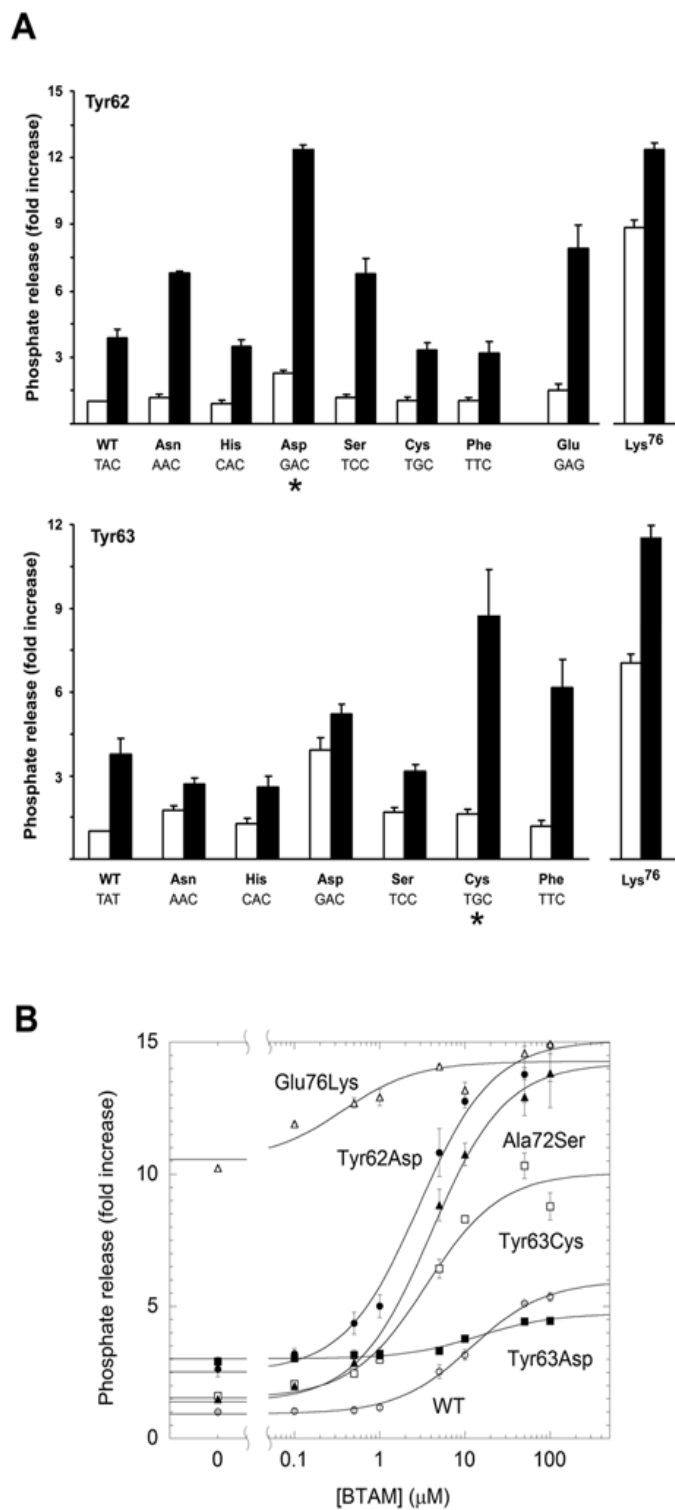


Figure 3. Biochemical characterization of SHP2 mutants.

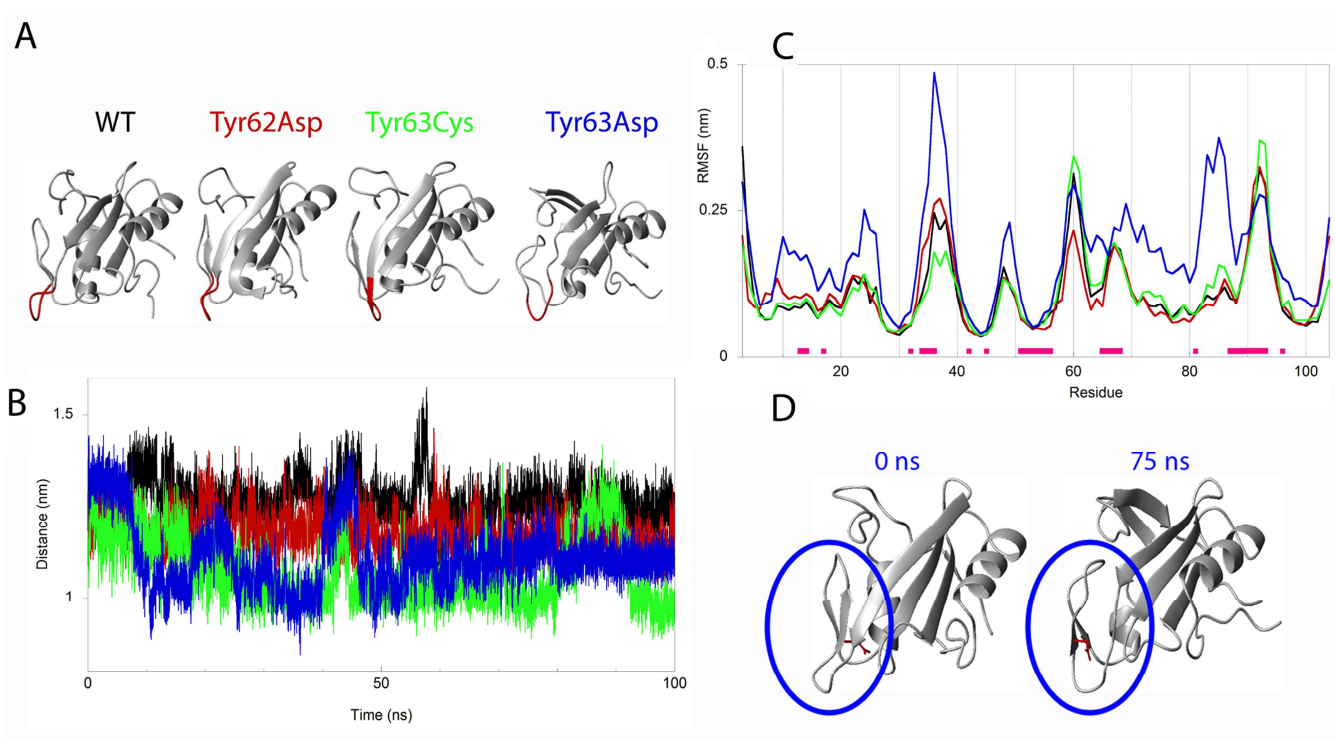


Figure 4. Molecular dynamics simulations.

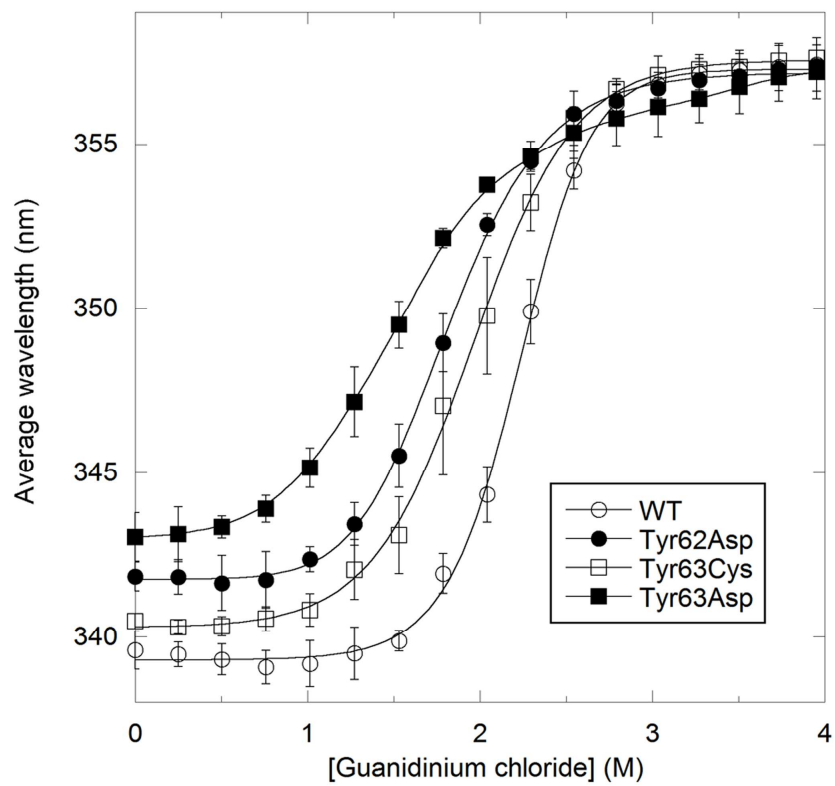


Figure 5. Chemical denaturation of the isolated wild-type and mutant N-SH2 domains, as indicated by the shift in the fluorescence spectrum of Trp⁶.

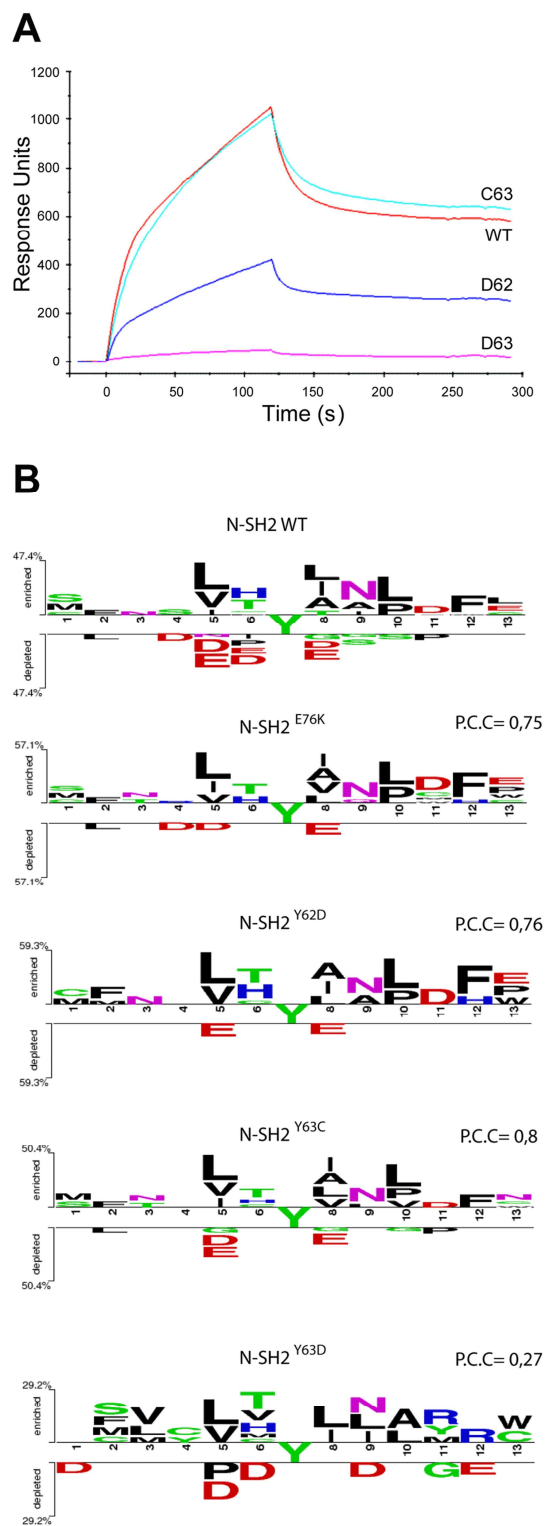


Figure 6. Phosphopeptide binding properties of wild-type and mutant N-SH2 domains.

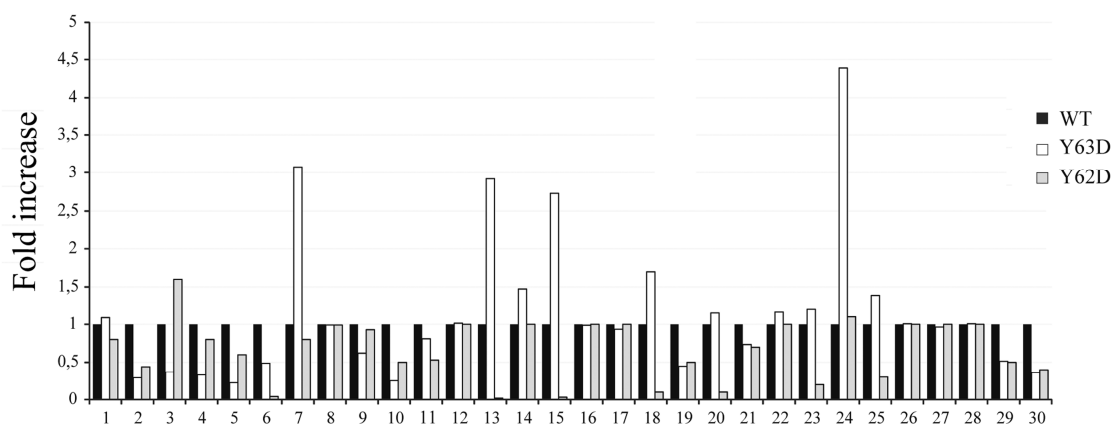
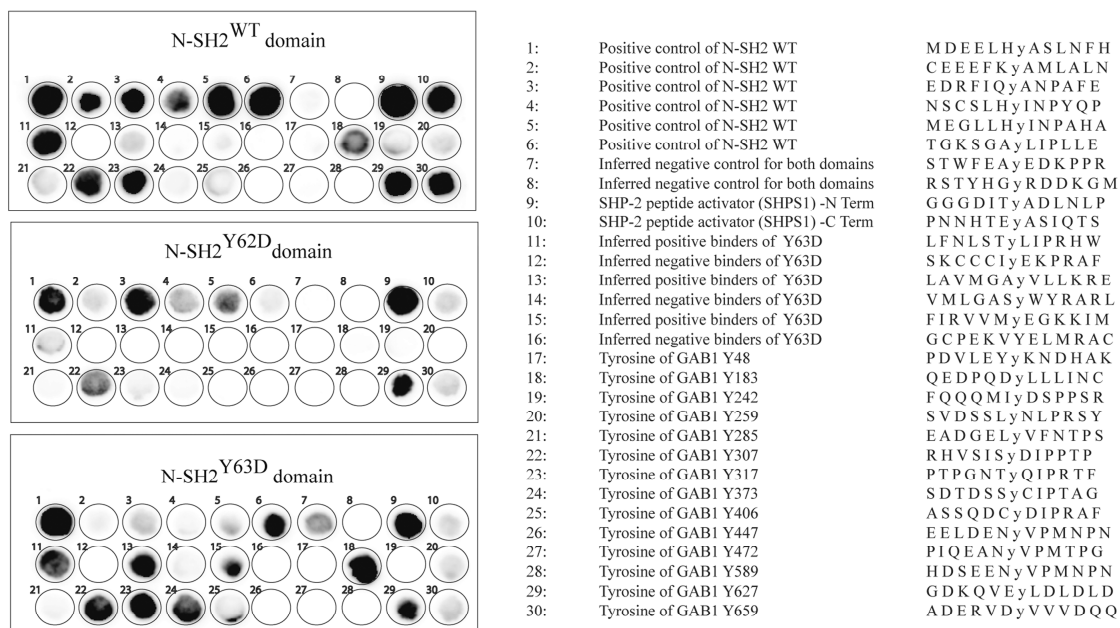


Figure 7. Phosphopeptide recognition specificity in SPOT synthesis assay.